Journal of
NANOSTRUCTURES
JNS
NANOSTRUCTURES
JNS.kashanu.ac.ir

Effects of Electro-Thermal Fields on Buckling of a Piezoelectric Polymeric Shell Reinforced with DWBNNTs

A. Ghorbanpour Arani*, S. Shams, S. Amir, Z. Khoddami Maraghi

Faculty of Mechanical Engineering, [b]Institute of Nanoscience & Nanotechnology,University of Kashan,Kashan, I.R.Iran.

Article history:
Received 22/7/2012
Accepted 25/11/2012
Published online 1/12/2012

Keywords:
Axial buckling
Boron Nitride Nanotube
Energy method
Electro-thermo-mechanical loadings

**Corresponding author:*
E-mail address*:*
aghorban@kashanu.ac.ir
Phone: +98 9131626594
Fax: +98 3615912424

Abstract

Using principle of minimum total potential energy approach in conjunction with Rayleigh-Ritz method, the electro-thermo-mechanical axial buckling behavior of piezoelectric polymeric cylindrical shell reinforced with double-walled boron-nitride nanotube (DWBNNT) is investigated. Coupling between electrical and mechanical fields are considered according to a representative volume element (RVE)-based micromechanical model. This study indicates how buckling resistance of composite cylindrical shell may vary by applying thermal and electrical loads. Also, applying the reverse voltage or decreasing the temperature, increases the critical axial buckling load. This work showed that the piezoelectric BNNT enhances on the whole the buckling resistance of the composite cylindrical shell.

1. Introduction

BNNTs, discovered in the mid 1990s [1-3], apart from similar properties to carbon nanotubes (CNTs) such as high chemical stability, excellent mechanical properties, and high thermal conductivity, offer higher temperature resistance to oxidation (>900 °C) [4,5], and piezoelectricity (not observed in CNTs). Compared with metallic or semiconducting CNTs, a BNNT is an electrical insulator with a band gap of ca. 5 eV, and hence independent of tube geometry; therefore it is more suitable for composite reinforcement than CNTs. Composites of BNNTs dispersed in ceramic or polymeric matrices have attracted a considerable attention in recent years due to their potential applications in aeronautic and astronautic technology, automobile, electronic and mechanical devices, and many other modern industries.

Haque and Ramasetty [6] developed an analytical model to study stress transfer in single-

walled carbon nanotubes (SWCNTs) reinforced polymer matrix composites. Their model can be used to predict axial stress and interfacial shear stress along the CNT embedded in matrix materials. The effects of CNT aspect ratio, CNT volume fraction and matrix modulus on axial stress and interfacial shear stress were also considered by [6] who compared their results of analytical model with those obtained from finite element analysis. Ghorbanpour Arani et al. [7] investigated the buckling analysis of laminated composite plates reinforced by SWCNTs using an analytical approach as well as the finite element method. Their developed model is based on the classical laminated plate theory (CLPT) and the third-order shear deformation theory for moderately thick laminated plates. They showed that agglomeration of CNTs have significant influence on the buckling load and properties of CNT reinforced composite. Odegard et al. [8] presented a technique for developing constitutive models for polymer composite systems reinforced with SWCNT. The modeling technique took into account the discrete nature of the atomic interactions at the nanometer length scale and the interfacial characteristics of the nanotube and the surrounding polymer matrix. Vodenitcharova and Zhang [9] studied the pure bending and bending-induced local buckling of a nanocomposite beam reinforced by a SWCNT. They found that in thicker matrix layers the SWNT buckles locally at smaller bending angles and greater flattening ratios.

Using a multiscale approach, a shear-lag model for evaluating the interfacial stress transfer in CNT reinforced polymer composites was studied by Gao and Li [10]. The carried out the continuum-based shear-lag analysis using the elasticity theory for axisymmetric problems, which results in closed-form formulas for predicting the interfacial shear stress and other axial stress components in both the nanotube and the matrix. Shen and Zhang [11] studied thermal post-buckling behavior of functionally graded carbon nanotube-reinforced composite plates subjected to in-plane temperature variation based on a micromechanical model and multi-scale approach. Their results indicated that the thermal post-buckling behaviors of CNT reinforced composite plates were significantly influenced by the thermal load ratio, the transverse shear deformation, the plate aspect ratio as well as the nanotube volume fraction. Salehi-Khojin and Jalili [12] studied the buckling of boron nitride nanotube reinforced piezoelectric polymeric composites subjected to combined electro-thermo-mechanical loadings. Their results indicated that the piezoelectric matrix enhanced the buckling resistance of composite significantly, and the supporting effect of elastic medium depended on the direction of applied voltage and thermal flow. Also, Salehi-Khojin and Jalili [13] proposed a semi-active control approach to obtain a composite structure with tunable mechanical properties ranging from stiffer structure to better damper. For this purpose, they proposed to apply an external electrical field to a piezoelectric polymeric matrix such as polyvinylidene fluoride (PVDF) reinforced with carbon nanotube. They showed that upon electrical loads to PVDF reinforced with nanotubes, the interfacial adhesion can be selectively controlled based on some desired characteristics.

Motivated by these considerations, this work aims to study the electro-thermo-mechanical axial buckling of a piezoelectric polymeric cylindrical shell reinforced with DWBNNTs. The present paper extends the principle of minimum potential energy to obtain the critical buckling load of symmetrically cylindrical composite shells with

two cases of boundary conditions: simple and clamp supports. Applying uniform electrical and thermal fields to a layer of PVDF shell reinforced by DWBNNTs, this work attempts to verify the influence of thermal and electrical loads on buckling resistance of cylindrical shell composites.

2. Governing equations

2. 1. Properties of piezoelectric polymeric composites

Effective properties of polymeric piezoelectric fiber reinforced composites (PPFRC) with square or rectangular piezoelectric fiber and unit cell cross-sections were obtained using RVE model [14]. The closed-form formula is derived using linear piezoelectric theory and iso-field assumptions under multiple loads including iso-strain, iso-stress, iso-electric field, and iso-electric displacement.

2. 2. Electro-Mechanical coupling

Considering that electro-mechanical behavior of the material is elastic and linear, the coupling between the corresponding mechanical and electrostatic fields will be limited to the linear case and is assumed as such. Also, stresses σ and strains ε on the mechanical side, as well as radial electric displacement D and electric field E on the electrostatic side, are arbitrarily combined according to [15] into two forms of coupled constitutive equations as follows:

$$\begin{Bmatrix}\sigma\\ D\end{Bmatrix}=\overbrace{\begin{bmatrix}C^E & -e\\ e^T & e^{\varepsilon}\end{bmatrix}}^{\mathbf{C}}\begin{Bmatrix}\varepsilon\\ E\end{Bmatrix},\quad \begin{Bmatrix}\varepsilon\\ D\end{Bmatrix}=\overbrace{\begin{bmatrix}S^E & d\\ d^T & \in^{\sigma}\end{bmatrix}}^{\mathbf{S}}\begin{Bmatrix}\sigma\\ E\end{Bmatrix}. \tag{1}$$

Therefore, constants of the matrices e and d correspond to induced stress and strain, respectively [15].

2. 3. Cylindrical shell theory

To model the assembly of layers or laminae of materials with piezoelectric properties, it has been suggested by [15] to extend the classical lamination theory for conventional laminates [16, 17]. In cylindrical shell theory, according to Kirchhoff–Love hypothesis, normal and shear strains transverse to the laminate are assumed to be negligibly small. Such deformations are expressed by the remaining strains as [15]:

$$\underbrace{\begin{Bmatrix}\varepsilon_x\\ \varepsilon_s\\ \gamma_{xs}\\ \bar{E}_1\end{Bmatrix}}_{\varepsilon}=\underbrace{\begin{Bmatrix}\varepsilon_x^0\\ \varepsilon_s^0\\ \gamma_{xs}^0\\ \bar{E}_1^0\end{Bmatrix}}_{\varepsilon^0}+n\underbrace{\begin{Bmatrix}\kappa_x\\ \kappa_s\\ \psi_{xs}\\ \bar{F}_1\end{Bmatrix}}_{\kappa}, \tag{2}$$

where ψ_{xs} is the curvature vector, and ε_x^0 is the middle-surface linear strain. As can be seen, strains and electric field intensity vary linearly through the laminate thickness with a constant portion ε^0 associated with the middle surface of the laminate and a linear portion $n\,k$. The stresses and radial electric displacement of the layer are hence determined as follows:

$$\begin{Bmatrix}\sigma_x\\ \sigma_s\\ \tau_{xs}\\ D_1\end{Bmatrix}=\bar{C}\begin{Bmatrix}\varepsilon_x\\ \varepsilon_s\\ \gamma_{xs}\\ \bar{E}_1\end{Bmatrix}, \tag{3}$$

where, σ_x and σ_s are normal stresses in *x* and *s* directions, respectively. τ_{xs} is the shear stress in *xs* plane. D_1 is the electrical displacement in direction 1(along cylinder axis), as indicated in Figure 1. Defining N and M as in-plane and out-of plane resultants, respectively, and using the appropriate subscript, for the overall structure, we have:

$$N = \begin{Bmatrix} N_x \\ N_s \\ N_{xs} \\ G_1 \end{Bmatrix} = \int_{-h/2}^{h/2} \begin{Bmatrix} \sigma_x \\ \sigma_s \\ \tau_{xs} \\ D_1 \end{Bmatrix} dn, \tag{4a}$$

$$M = \begin{Bmatrix} M_x \\ M_s \\ M_{xs} \\ H_1 \end{Bmatrix} = \int_{-h/2}^{h/2} n \begin{Bmatrix} \sigma_x \\ \sigma_s \\ \tau_{xs} \\ D_1 \end{Bmatrix} dn. \tag{4b}$$

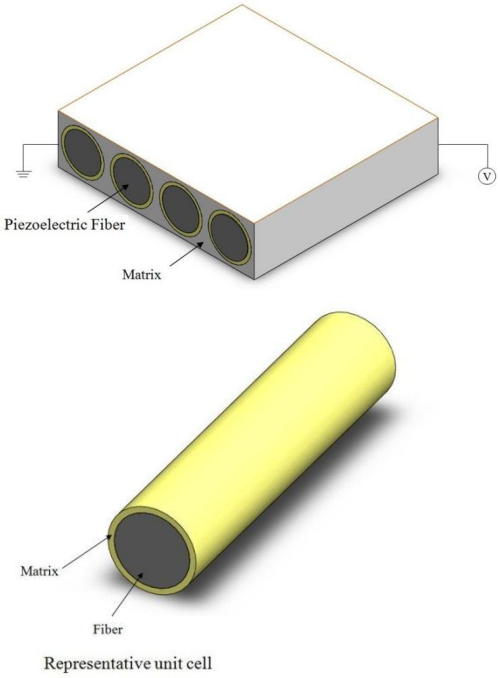

Fig. 1. A schematic of RVE and DWBNNTs reinforced composite.

2. 4. Strain displacement relations

In order to calculate the middle-surface strain and curvatures, using Kirchhoff-Love assumtions, the displacement components of an arbitrary point anywhere are written as [18]:

$$\begin{aligned} u(x,s,z) &= u_0(x,s) - z\frac{\partial w(x,s)}{\partial x}, \\ v(x,s,z) &= v_0(x,s) - z\frac{\partial w(x,s)}{\partial s}, \\ w(x,s,z) &= w_0(x,s). \end{aligned} \tag{5}$$

However, middle-surface strains and curvatures could be defined by applying Koiter–Sanders strain–displacement relationships [15] or Donnell's formulation [19] as follows:

$$\varepsilon_x^0 = \frac{\partial u_0}{\partial x},\ \varepsilon_s^0 = \frac{\partial v_0}{\partial s} + \frac{w}{R},\ \gamma_{xs}^0 = \frac{\partial v_0}{\partial x} + \frac{\partial u_0}{\partial s}, \tag{6a}$$

$$k_x = -\frac{\partial^2 w}{\partial x^2},\ k_s = -\frac{\partial^2 w}{\partial s^2} + \frac{\partial}{\partial s}\left(\frac{v_0}{R}\right), \tag{6b}$$

$$\psi_{xs} = -2\frac{\partial^2 w}{\partial x\,\partial s} + \frac{\partial}{\partial x}\left(\frac{v_0}{R}\right) + \frac{1}{2R}\left(\frac{\partial v_0}{\partial x} - \frac{\partial u_0}{\partial s}\right), \tag{6c}$$

where k_x and k_s are curvatures in the axial and circumferential direction, respectively. It should be noted that in the cylindrical coordination $S = R\varphi$ denotes the arc length S, the radius R and azimuth of φ.

3. Buckling analysis

3. 1. Total potential energy

Total potential energy for an elastic body is expressed as [20]:

$$V = U - \int_{s_r} T_i u_i dS - \int_V F_i u_i dV, \tag{7}$$

where, the 1st term on right hand side is electrostatic energy. The 2nd and 3rd terms represent the work done by the surface tractions and the body forces, respectively. The electroelastic energy density determined generally as [15]:

$$u_0 = u_0^{md} - u_0^{ep},$$

where u_0^{md} is the strain energy density and u_0^{ep} is the electrical potential energy density [18]. Integrating over the entire structure gives the electroelastic energy, i.e.:

$$U = \frac{1}{2}\left[\int_\Lambda \varepsilon^T \sigma\, dV - \int_\Lambda E^T D\, dV\right]$$

Substituting Equation (4) into Equation (9), we have

$$\frac{1}{2}\int_{\Lambda}\left\{\varepsilon^{T} \quad \overline{E}^{T}\right\}\begin{Bmatrix}\sigma\\ D\end{Bmatrix}dV \tag{10}$$

Assuming uniform electrical fields, Equation (10) becomes

$$U=\frac{1}{2}\int_{\Lambda}\left\{\varepsilon_x \quad \varepsilon_s \quad \gamma_{xs} \quad \overline{E}_1\right\}\begin{bmatrix}\overline{C}_{11} & \overline{C}_{12} & 0 & e_{11}\\ \overline{C}_{12} & \overline{C}_{22} & 0 & e_{12}\\ 0 & 0 & \overline{C}_{66} & 0\\ e_{11} & e_{12} & 0 & -\in_{11}\end{bmatrix}\begin{Bmatrix}\varepsilon_x\\ \varepsilon_s\\ \gamma_{xs}\\ \overline{E}_1\end{Bmatrix}dV, \tag{11}$$

where $\overline{C}_{ij}$, e_{ij}, and $\in_{ij}$ are the off-axis elastic coefficients of composites in coordinate system of shell, piezoelectric constants and dielectric constants, respectively, i.e.:

$$\begin{aligned}
\overline{C_{11}} &= C_{11}\cos^4\theta + 2(C_{12}+2C_{66})\sin^2\theta\cos^2\theta + C_{22}\sin^4\theta,\\
\overline{C_{12}} &= (C_{11}+C_{22}-4C_{66})\sin^2\theta\cos^2\theta + C_{12}(\sin^4\theta+\cos^4\theta),\\
\overline{C_{22}} &= C_{11}\sin^4\theta + 2(C_{12}+2C_{66})\sin^2\theta\cos^2\theta + 2C_{22}\cos^4\theta,\\
\overline{C_{66}} &= (C_{11}+C_{22}-2C_{12}-2C_{66})\sin^2\theta\cos^2\theta + C_{66}(\sin^4\theta+\cos^4\theta),
\end{aligned} \tag{12}$$

where C_{ij} are the on-axis elastic coefficients of composites. θ denotes the angle between local and global coordinate systems. Substituting Equation (4) into Equation (1) yields:

$$\varepsilon_x = \frac{\partial u_0}{\partial x} - z\,\frac{\partial^2 w}{\partial x^2}, \tag{13a}$$

$$\varepsilon_s = \frac{\partial v_0}{\partial s} + \frac{w}{R} + z\left(-\frac{\partial^2 w}{\partial s^2} + \frac{\partial}{\partial s}\left(\frac{v_0}{R}\right)\right), \tag{13b}$$

Axial and circumferential middle-plane displacements in x and s directions are negligible. Also, stress and strain in thickness direction are ignored. Therefore, Equations (13) are simplified as follows:

$$\varepsilon_x = -z\,\frac{\partial^2 w}{\partial x^2}, \tag{14a}$$

$$\varepsilon_s = \frac{w}{R} - z\,\frac{\partial^2 w}{\partial s^2}, \tag{14b}$$

$$\gamma_{xs} = -2z\,\frac{\partial^2 w}{\partial x\,\partial s}. \tag{14c}$$

Applying matrix multiplication on Equation (11) gives:

$$U=\frac{1}{2}\int_{\Lambda}\begin{pmatrix}\overline{C}_{11}\varepsilon_x^2 + 2\overline{C}_{12}\varepsilon_s\varepsilon_x + 2\overline{E}_1 e_{12}\varepsilon_s + \overline{C}_{22}\varepsilon_s^2\\ +2\overline{E}_1 e_{11}\varepsilon_x + \overline{C}_{66}\gamma_{xs}^2 - \in_{11}\overline{E}_1^2\end{pmatrix}dV. \tag{15}$$

Substituting Equations (14) into Equation (15) gives the electrostatic energy as:

$$U=\frac{1}{2}\int_{A}\begin{pmatrix}\overline{C}_{11}\left(-n\frac{\partial^2 w}{\partial x^2}\right)^2 + 2\overline{C}_{12}\left(-n\frac{\partial^2 w}{\partial x^2}\right)\left(\frac{w}{R}-n\frac{\partial^2 w}{\partial s^2}\right)\\ +2\overline{E}_1 e_{11}\left(-n\frac{\partial^2 w}{\partial x^2}\right)+\overline{C}_{22}\left(\frac{w}{R}-n\frac{\partial^2 w}{\partial s^2}\right)^2\\ +2\overline{E}_1 e_{12}\left(\frac{w}{R}-n\frac{\partial^2 w}{\partial s^2}\right)+\overline{C}_{66}\left(-2n\frac{\partial^2 w}{\partial x\,\partial s}\right)^2\\ -\in_{11}\overline{E}_1^2\end{pmatrix}dV \tag{16}$$

Work done by traction forces are expressed as [21]:

$$\int_{Sr} T_i u_i dS = \int_0^{2\pi}\int_0^{L} N_x\left[\frac{\partial u_0}{\partial x} + \frac{1}{2}\left(\frac{\partial w}{\partial x}\right)^2\right]R\,dx\,d\varphi, \tag{17}$$

where N_x is applied axial force on two edges of cylinder which is defined as:

$$\begin{aligned}
N_x &= N_x^{mech} + N_x^{T} + N_x^{E},\\
N_{ij}^{T} &= \int_{-\frac{h}{2}}^{\frac{h}{2}}(\overline{C}_{ij})\left[\alpha_{ij}\right]_k\,\Delta T\,dz,\\
N_{ij}^{E} &= \int_{-\frac{h}{2}}^{\frac{h}{2}}(e_{ij})\left[\overline{E}_{ij}\right]_k\,dz,
\end{aligned} \tag{18}$$

where N_x^{mech}, N_x^{T} and N_x^{E} are mechanical, thermal and electrical forces, respectively. Using Equation (7), the total potential energy of the composite shell is obtained as:

$$
\begin{aligned}
&V\,\frac{1}{2}\int_0^{2\pi}\int_0^{L}[\bar{C}_{11}\left(\frac{(R+h)^3-R^3}{3}\left(\frac{\partial^2 w}{\partial x^2}\right)^2+h\left(\alpha_x\Delta T\right)^2+\right.\\
&\left.\left((R+h)^2-R^2\right)\frac{\partial^2 w}{\partial x^2}\alpha_x\Delta T\right)\\
&+2\bar{C}_{12}\left(-\left((R+h)^2-R^2\right)\frac{\partial^2 w}{\partial x^2}\frac{w}{2R}+\frac{(R+h)^3-R^3}{3R^2}\frac{\partial^2 w}{\partial x^2}\frac{\partial^2 w}{\partial\theta^2}\right.\\
&\bar{C}_{11}\left(\frac{(R+h)^3-R^3}{3}\left(\frac{\partial^2 w}{\partial x^2}\right)^2+h\left(\alpha_x\Delta T\right)^2+\left((R+h)^2-R^2\right)\frac{\partial^2 w}{\partial x^2}\alpha_x\Delta T\right)\\
&+2\bar{C}_{12}\left(-\left((R+h)^2-R^2\right)\frac{\partial^2 w}{\partial x^2}\frac{w}{2R}+\frac{(R+h)^3-R^3}{3R^2}\frac{\partial^2 w}{\partial x^2}\frac{\partial^2 w}{\partial\theta^2}\right.\\
&+\frac{(R+h)^2-R^2}{2}\alpha_\theta\Delta T\,\frac{\partial^2 w}{\partial x^2}-\alpha_x h\Delta T\,\frac{w}{R}+\left((R+h)^2-R^2\right)\frac{\alpha_x\Delta T}{2R^2}\frac{\partial^2 w}{\partial\theta^2}\\
&+\alpha_x\alpha_\theta h\Delta T^2-2\bar{E}_1 e_{11}\left(\frac{(R+h)^2-R^2}{2}\frac{\partial^2 w}{\partial x^2}+\alpha_x h\Delta T\right)+\\
&\bar{C}_{22}\left(\left(\frac{w}{R}\right)^2 h+\frac{(R+h)^3-R^3}{3R^4}\left(\frac{\partial^2 w}{\partial\theta^2}\right)^2+h\left(\alpha_\theta\Delta T\right)^2-\left((R+h)^2-R^2\right)\frac{w}{R^3}\frac{\partial^2 w}{\partial\theta^2}\right.\\
&\left.-2\frac{w}{R}h\alpha_x\Delta T+\frac{(R+h)^2-R^2}{R^2}\frac{\partial^2 w}{\partial\theta^2}\alpha_\theta\Delta T\right)+\\
&2\bar{E}_1 e_{12}\left(\frac{hw}{R}-\frac{(R+h)^2-R^2}{2R^2}\frac{\partial^2 w}{\partial\theta^2}-\alpha_\theta h\Delta T\right)+\bar{C}_{66}\left(\frac{4\left((R+h)^3-R^3\right)}{3R^2}\left(\frac{\partial^2 w}{\partial x\,\partial\theta}\right)^2\right.\\
&\left.\left.+h\left(\alpha_{x\theta}\Delta T\right)^2+\frac{2\left((R+h)^2-R^2\right)\alpha_{x\theta}}{R}\Delta T\,\frac{\partial^2 w}{\partial x\,\partial\theta}\right)-\epsilon_{11}\bar{E}_1^2 h\right]R\,dx\,d\theta\\
&-\frac{1}{2}\int_0^{2\pi}\int_0^{L}\left[N_x+(\bar{C}_{11}\alpha_x+\bar{C}_{12}\alpha_\theta)h\Delta T+e_{11}\bar{E}_1 h\right]\left(\frac{\partial w}{\partial x}\right)^2 R\,dx\,d\theta,
\end{aligned}
\tag{19}
$$

where, R and L are radius and length of the shell, respectively.

3. 2. Boundary conditions

In this article, two boundary conditions for cylindrical composite shell are considered; Case 1 referring to a shell simply supported on two edges and Case 2 referring to a shell with edges being clamped on both sides. These boundary conditions are described mathematically as follows:

Case 1) Simply supported

$$
\begin{aligned}
&w=0; \quad \text{at} \quad x=0 \text{ and } L,\\
&\frac{\partial^2 w}{\partial x^2}=0; \quad \text{at} \quad x=0 \text{ and } L.
\end{aligned}
\tag{20}
$$

For satisfying these conditions, the following function is assumed for the lateral displacement

$$
w=\sum_{p=1}^{\infty}\sum_{q=1}^{\infty}A_{pq}\sin\left(\alpha_p x\right)\cos\left(q\theta\right),\ \alpha_p=\frac{p\pi}{L},
\tag{21}
$$

where p and q are axial half and circumferential wave-numbers, respectively.

Case2) Clamped support

$$
\begin{aligned}
&w=0; \quad \text{at} \quad x=0 \text{ and } L,\\
&\frac{\partial w}{\partial x}=0; \quad \text{at} \quad x=0 \text{ and } L.
\end{aligned}
\tag{22}
$$

Similarly, the following function is assumed to describe the lateral displacement

$$
w=\sum_{p=1}^{\infty}\sum_{q=1}^{\infty}A_{pq}\left(1-\cos 2\alpha_p x\right)\cos(q\theta),\ \alpha_p=\frac{p\pi}{L}.
\tag{23}
$$

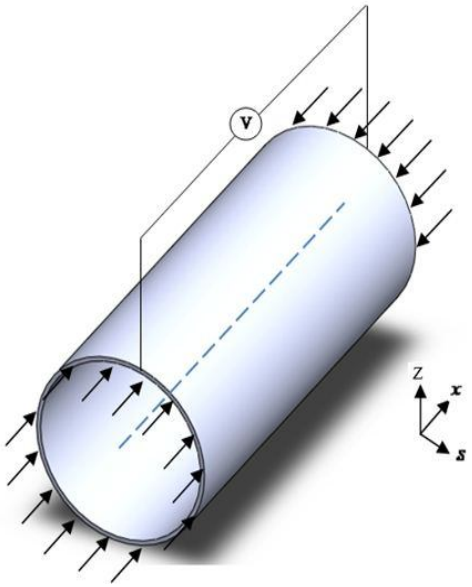

Fig. 2. Hollow circular cylindrical composite shell with axial load and applied voltage V .

3. 3. Minimum total potential energy method

According to the definition of minimum potential energy, of all the displacements satisfying compatibility and the prescribed boundary conditions, those that satisfy the equilibrium equations make the potential energy a minimum [20]. Mathematically, this happens when $\delta V = 0.$

Substituting the lateral displacement in total potential energy and applying minimum potential energy principle, the axial buckling force of composite shells may be expressed as below for the two cases of boundary conditions stated above:

Case 1:

$$N_x = \bar{C}_{11}\left(\alpha_p^2 \frac{(R+h)^3 - R^3}{3}\right) + 2\bar{C}_{12}\left(\frac{(R+h)^2 - R^2}{2R} + q^2 \frac{(R+h)^3 - R^3}{3R^2}\right) + \frac{\bar{C}_{22}}{\alpha_p^2}\left(\frac{h}{R^2} + q^4 \frac{(R+h)^3 - R^3}{3R^4} + q^2 \frac{(R+h)^2 - R^2}{R^3}\right) + \bar{C}_{66}\left(q^2 \frac{4\left((R+h)^3 - R^3\right)}{3R^2}\right) - (\bar{C}_{11}\alpha_x + \bar{C}_{12}\alpha_\theta)h\Delta T - e_{11}\bar{E}_1 h. \quad (24)$$

Case 2:

$$N_x = \bar{C}_{11} 4\alpha_p^2 \frac{(R+h)^3 - R^3}{3} + \bar{C}_{12}\left(\frac{(R+h)^2 - R^2}{R} + 2q^2 \frac{(R+h)^3 - R^3}{3R^2}\right) + \frac{\bar{C}_{22}}{\alpha_p^2}\left(\frac{3h}{4R^2} + q^4 \frac{(R+h)^3 - R^3}{12R^4} + 3q^2 \frac{(R+h)^2 - R^2}{4R^3}\right) + 4\bar{C}_{66} q^2 \frac{\left((R+h)^3 - R^3\right)}{3R^2} - (\bar{C}_{11}\alpha_x + \bar{C}_{12}\alpha_\theta)h\Delta T - e_{11}\bar{E}_1 h. \quad (25)$$

4. Numerical result and discussion

In this section, numerical results on the effects of thermal and electrical loads on axially compressed buckling of the piezoelectric cylindrical shell are investigated. Using modeling procedure described above and Equations (24- 25), the numerical results of the critical buckling load are demonstrated in Figures 2 to 6. The nanotube considered as fiber in this study is DWBNNT, with the zigzag structure, has Young's modulus E = 1.8 TPa, the axial and circumferential thermal expansion coefficients ($\alpha_x = 1.2e-6$ and $\alpha_\varphi = 0.6e-6$) and piezoelectric constant $e_{11} = 0.95 C/m^2$. The properties of PVDF considered as matrix are: $C_{11} = 238.24 GPa$, $C_{22} = 23.6 GPa$, $C_{66} = 6.43 GPa$, $C_{12} = 3.98 GPa$, $e_{11} = -0.13 C/m^2$, and $\alpha = 7.1e-5 \frac{1}{^\circ C}$. The dimensional properties of the shell considered are: R =246.2 nm and the thickness of the shell equals to thickness of single layer of nanocomposite which depends on BNNTs volume fraction. Temperature change and applied voltage are $100\,^\circ C$ and 25 V, respectively [12, 13].

Buckling occurs for the minimum load, i.e. the critical axial buckling load ($N_{x\text{-crit}}$). Figures 2 show axial buckling load (N_x) as a function of axial half wave-number (p) under mechanical load for the two cases of boundary conditions. As can be seen N_x depends on the fiber volume fraction (ρ) but its influence decreases for higher incremental increase in ρ. However, it is worth noting that the effect of ρ on N_x is different prior and post the minimum load. Before $N_{x\text{-crit}}$, maximum N_x corresponds to maximum ρ, while after $N_{x\text{-crit}}$ this behavior is reversed. As far as the simple and clamped boundary conditions are concerned, generally in the former, $N_{x\text{-crit}}$ is smaller in magnitude, indicating the importance of the boundary conditions on the two edges under critical axial buckling load of the cylindrical shell.

Figures 3 show N_x as a function of circumferential wave-number (q). Buckling takes place in the first circumferential half wave number where the minimum occurs around 20000 to 25000

N/m range for all ρ considered here. After the minimum, N_x tends to increase with q with the slope being increased continuously for higher q. Dependency of $N_{x\text{-}crit}$ on ρ can also be reconfirmed here as in Figures 2.

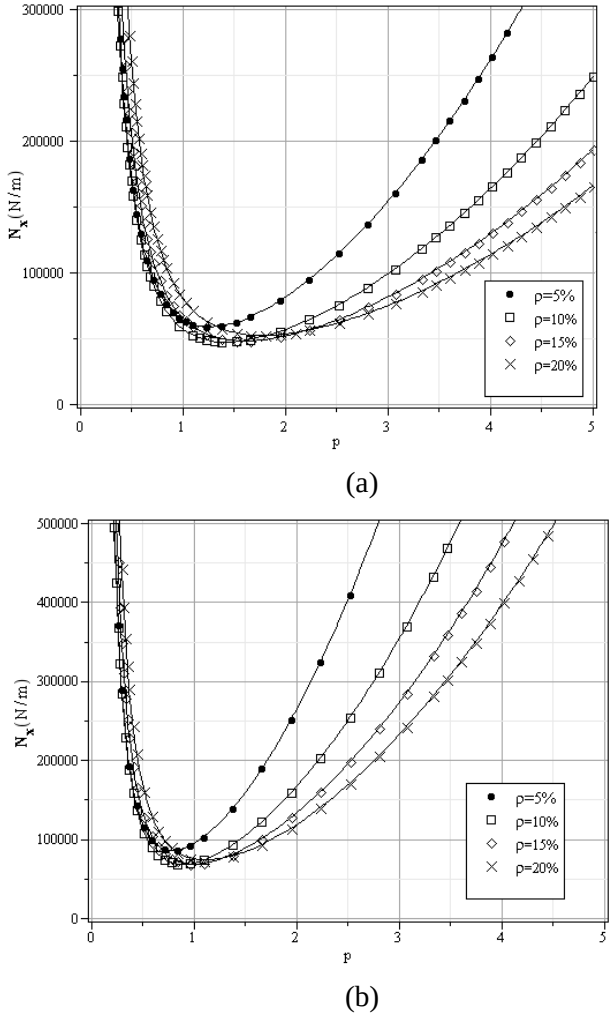

Fig. 3. Axial buckling load, versus axial half wave-number p for (a) simple support, and (b) clamped support.

Figures 4 illustrate axial buckling load, N_x, as a function of axial half wave number, p, under mechanical loading. $N_{x\text{-}crit}$ increases with increase in q. Also, N_x increases with increasing q for a constant p.

The axial buckling load as a function of aspect ratio (L/R) is shown in Figures 5. The critical axial buckling load is almost independent of the axial half wave numbers considered here and is about 60,000 N/m and 85,000 N/m for simple and clamped support boundary conditions, respectively.

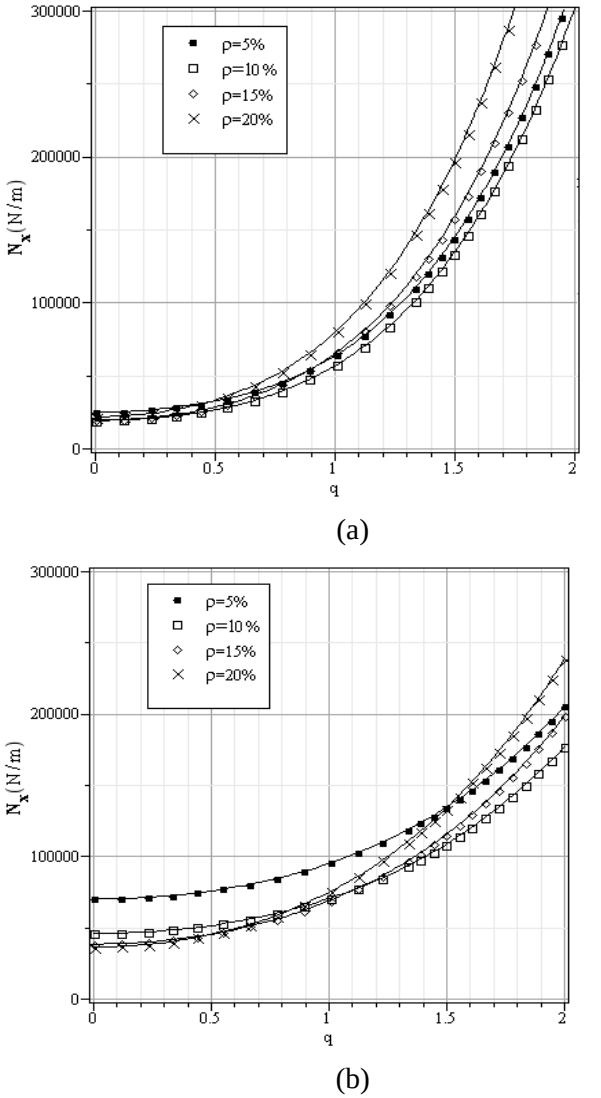

Fig. 4. Axial buckling load, versus circumferential wave-number q for (a) simple support, and (b) clamped support.

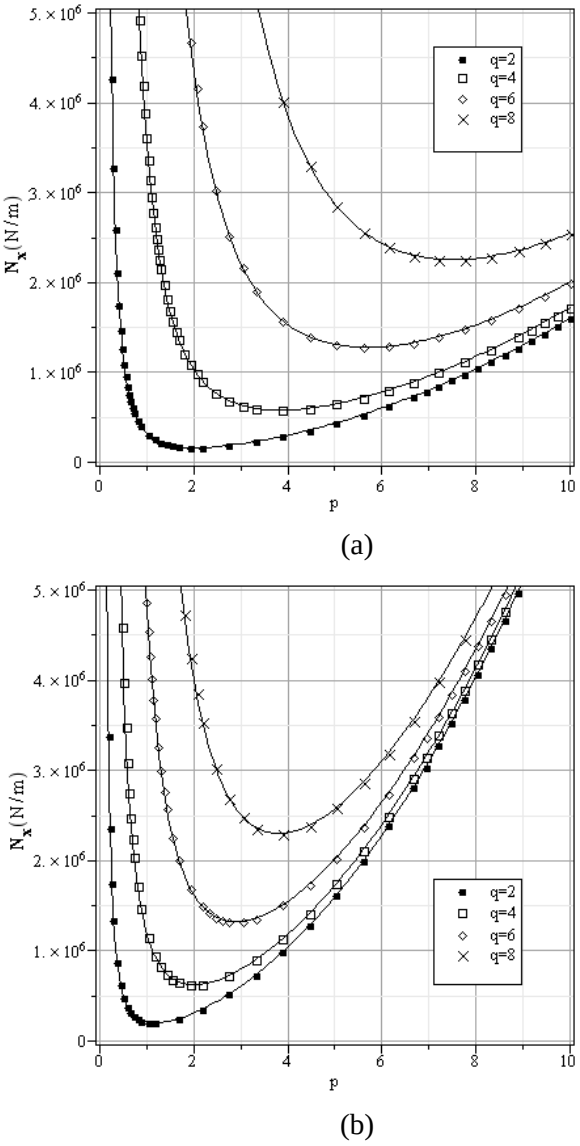

Fig. 5. Axial buckling load, versus circumferential wave-number p for (a) simple support, and (b) clamped support.

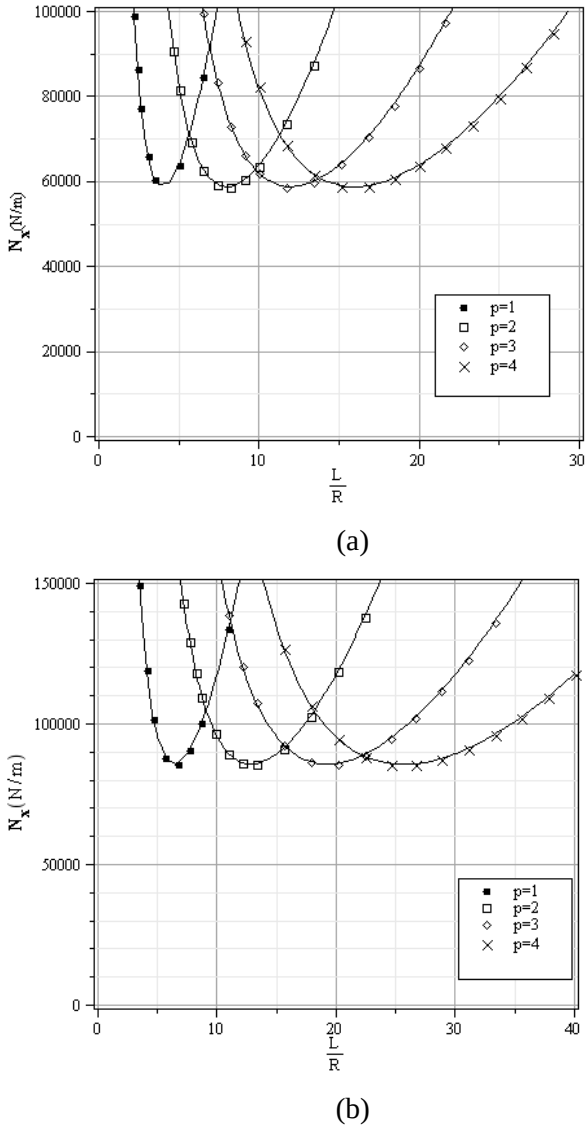

Fig. 6. Axial buckling load, versus shell aspect ratio (a) simple support, and (b) clamped support for $q=1$.

Figures 6 show the combined and isolated effects of thermal, electrical as well as mechanical fields. Applying reverse voltage, increases Nx-crit irrespective of the wave numbers employed, perhaps due to polarization created in the piezoelectric in the longitudinal direction leading to its contraction [12].

This makes piezoelectric structure stronger and more compact in loading direction. Similar results are achieved when shell temperature is reduced. This results conforms the findings of Salehi-Khojin and Jalili [12] who believes that the electrical load is more efficient and more effective than the thermal one possibly due to the faster response of piezoelectric shell to the former. It should be noted that as far as potential applications are concerned,

applying electrical field to piezoelectric is easier and more beneficial.

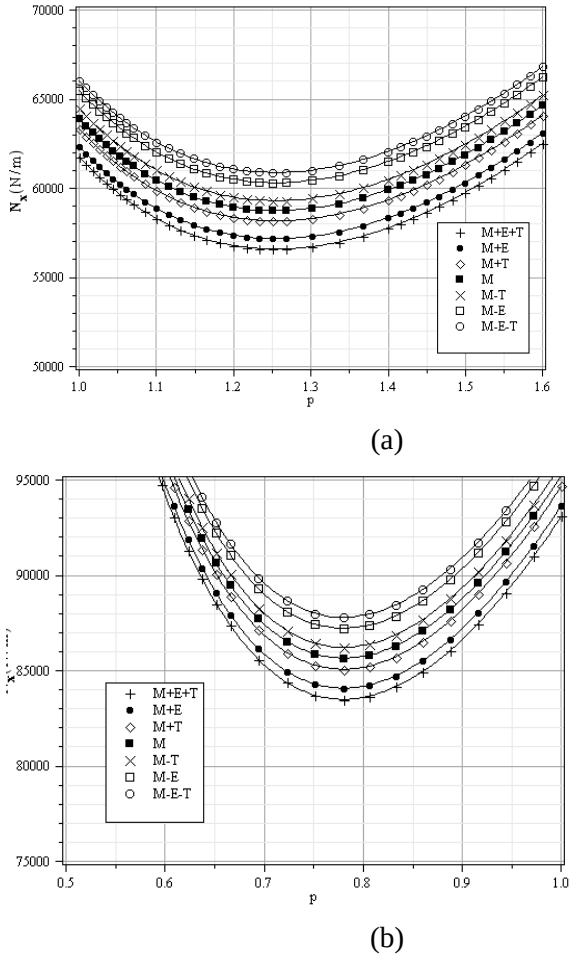

Fig. 7. Axial buckling load, versus axial half wave number for (a) simple support, and (b) clamped support.

5. Conclusions

In this study, minimum total potential energy approach is used to evaluate the axial buckling load behavior in a piezoelectric polymeric cylindrical shell reinforced with DWBNNT subjected to combined electro-thermo-mechanical loadings. Classical boundary conditions of simple and clamped supports are considered for this. Coupling between electrical and mechanical fields are considered according to a RVE-based micromechanical model. The results indicate that the influence of volume fiber fraction decreases for higher incremental increase in ρ. As far as the simple and clamped boundary conditions are concerned, generally in the former, $N_{x\text{-}crit}$ is smaller in magnitude, indicating the importance of the boundary conditions on the two edges under critical axial buckling load of the cylindrical shell. The axial buckling load is almost independent of the axial half wave numbers when it plotted versus the aspect ratio. The critical axial buckling load occurs for $q=1$. It is shown that buckling resistance of composite cylindrical shell varies by applying thermal and electrical loads. Applying the reverse voltage or decreasing the temperature, increases the critical axial buckling load. Results obtained in this study indicate that piezoelectric BNNT enhances the buckling resistance of the composite cylindrical shell.

Acknowledgement

The authors are grateful to University of Kashan for supporting this work by Grant No. 65475/22. They would also like to thank the Iranian Nanotechnology Development Committee for their financial support.

References

[1] Rubio, J. L. Corkill, M. L. Cohen, Phys. Rev. B: Condens. Matter, 49 (1994) 5081.

[2] X. Blasé, A. Rubio, S. G. Louie, M. L. Cohen, Europhys. Lett., 28 (1994) 335.

[3] N. G. Chopra, R. J. Luyken, K. Cherrey, V. H. Crespi, M. L. Cohen, S. G. Louie, A. Zettl, Science, 269 (1995) 966.

[4] Y. Chen, J. Zou, S. J. Campbell, G. L. Caer, Appl. Phys. Lett., 84 (2004) 2430.

[5] N. Sai, E. J. Mele, Phys. Rev. B: Condens. Matter, 68 (2003) 241405.

[6] Haque, A. Ramasetty, Compos. Struct., 71 (2005) 68.
[7] A. Ghorbanpour Arani, Sh. Maghamikia, M. Mohammadimehr, A. Arefmanesh, J. Mech. Sci. Technol., 25 (2011) 809.
[8] G. M. Odegard, T. S. Gates, K. E. Wise, C. Park, E. J. Siochi, Compos. Sci. Technol., 63 (2003) 1671.
[9] T. Vodenitcharova, L. C. Zhang, Int. J. Solids Struct., 43 (2006) 3006.
[10] X. L. Gao, K. Li, Int. J. Solids Struct., 42 (2005) 1649
[11] H. S. Shen, C. L. Zhang, Mater. Des., 31 (2010) 3403.
[12] A. Salehi-Khojin, N. Jalili, Compos. Sci. Technol., 68 (2008) 1489.
[13] A. Salehi-Khojin, and N. Jalili, Composites Part B Engineering, 39 (2008) 986.
[14] P. Tan, L. Tong, Compos. Sci. Technol., 61 (2001) 759.
[15] T. H. Brockmann, Theory of adaptive fiber composites from piezoelectric material behavior to dynamics of rotating structures, Springer: USA; 2009.
[16] R. M. Jone, Mechanics of Composite Materials. Scripta Book Company: Washington; 1975.
[17] J. M. Whitney, Structural Analysis of Laminated Anisotropic Plates. Technomic Publishing Company: Lancaster; 1987.
[18] J. L. Sanders, An improved first-approximation theory for thin shells. Technical Report NASA TR R-24, National Aeronautics and Space Administration: Langley Research Center; 1959.
[19] W. T. Koiter. A consistent first approximation in the general theory of thin elastic shells. In Proceedings of the Symposium on the Theory of Thin Elastic Shells. Internation Union of Theoretical and Applied Mechanics North-Holland: Amsterdam; 1960.
[20] J. R. Vinson, Plate and Panel Structures of Isotropic, Composite and Piezoelectric Materials, Including Sandwich Construction, Springer: USA; 2005.
[21] L. H. Donnell, Stability of thin-walled tubes under torsion. Technical Report NACA Report No. 479: National Advisory Committee for Aeronautics; 1933.